An Accurate UWB Radar Imaging Method Using Indoor Multipath Echoes for Targets in Shadow Regions

Shuhei Fujita, Takuya Sakamoto and Toru Sato
Graduate School of Informatics, Kyoto University, Yoshida-Honmachi, Sakyo-ku, Kyoto 606-8501, Japan. Email: tsato@kuee.kyoto-u.ac.jp

***Abstract*—Ultra Wide-Band (UWB) pulse radar provides promise for surveillance systems via its high-range resolution. To realize a low-cost and high-quality indoor security system, we propose a UWB radar imaging system using indoor multipath echoes for targets in shadow regions. A multipath wave can be used as an approximation of an imaginary echo from a mirror image antenna to the target, ignoring phase rotation and attenuation. Conventional studies have only dealt with locating point-like targets, not estimating their shape. We apply interferometry using these mirror image antennas to estimate target shapes. If this method alone is applied, many false image points are estimated because it is difficult to determine uniquely the corresponding mirror image antenna to each echo. We propose an effective false-image reduction algorithm to obtain a clear image. Numerical simulations show that most of the false image points are removed and the target shape is accurately estimated.**

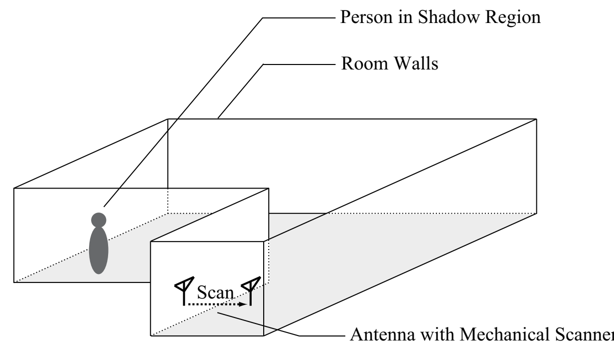

Fig. 1. Overview of surveillance system using UWB pulse radar.

I. Introduction

In anticipation of an increasingly aging society, monitoring systems for aged care are attracting attention. Most of the current monitoring/security systems use cameras because of their low-cost and high resolution capabilities. However, optical cameras have serious privacy-related problems. The introduction of infrared cameras is another candidate for monitoring systems because they are unlikely to capture surface textures thus reducing privacy concerns. In general, numerous cameras are needed to cover a total given area without any blind spots, making the entire system complicated and costly. A system using radiowaves is a promising candidate for this purpose as it has the potential to resolve some of the substantial problems of camera-based systems. Moreover, it has been reported that radiowaves enable the detection of targets in hidden places. Existing communication infrastructures like Wireless LAN (WLAN) stations have been employed for positioning purposes [1], [2]. Although these methods are capable of estimating target locations, an accurate target shape cannot be obtained.

To obtain the target's shape in addition to its location, a UWB pulse radar has great potential because of its high range resolution. However, most of the conventional algorithms, including SAR [3], [4], provide a target image for which the resolution is limited to half the wavelength. The SEABED algorithm [5], [6], [7] is another approach making use of the reversible transform between a received signal and the target boundary, which can produce images with a resolution much higher than any conventional algorithms. However, this algorithm assumes direct echoes, not multi-path echoes, and thus cannot be applied to a target in a blind spot. Furthermore, a new approach using multipath echoes, the time reversal (TR) method [8], [9], makes it possible to calculate an image using only a single antenna [10], [11]. Assuming a point-like target in a room of known shape, this method back-propagates the received signal numerically to focus on an image at the target location. The method cannot estimate a target's shape although it gives an accurate target location.

In this paper, we propose a new imaging method for UWB radar using a single antenna with a mechanical scanner that combines the ideas of the TR and the interferometry method [12] to accurately estimate a target shape in a multipath environment. This method also has a particular advantage over conventional camera-based systems because it enables the imaging of a target in an area that is out of sight. The proposed method picks up multipath echoes from the received signals to estimate the target shape. The procedure gives a correct target shape with many undesirable false images caused by the ambiguity of the propagation paths corresponding to multipath echoes in the received signals. To eliminate these false images, we propose an effective false image reduction algorithm to obtain a clear image. First, we explain the procedure of the proposed imaging method, followed by some numerical

978-1-4244-5864-6/10$26.00 © IEEE

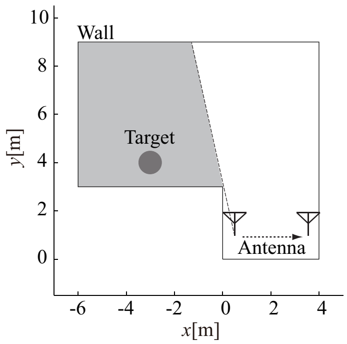

Fig. 2. System model A with a shadow region.

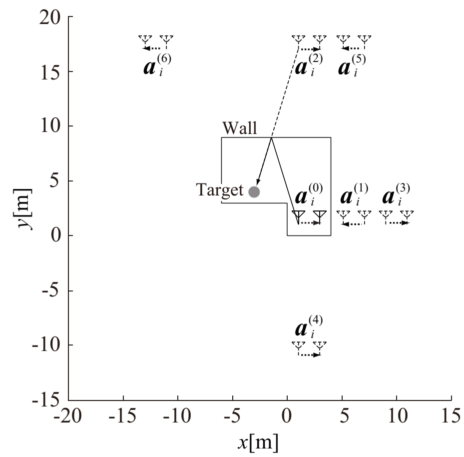

Fig. 3. Mirror image points for model A.

simulation results to show the performance of the proposed method compared with conventional methods.

II. System Model

For simplicity, we deal with a 2-dimensional problem in this paper. It is assumed that a radar system is installed on a mechanical scanner in a room as in Fig. 1. We assume that the room is configured as a known polygonal shape. A human target is located at an unknown position in the room. The room has a blind area blocked by walls. In this paper, the areas that cannot receive direct waves from the antenna are called shadow regions. Figure 2 shows an example of the shadow regions blocked by a wall in a room.

Figure 3 shows a model of the system, where an antenna and a circular target are located in an L-shaped room. In an ideal environment, the target and the room are made of perfect electric conductor (PEC) material. We define real space as the space where the target and antenna are located. We express real space with the parameters $\boldsymbol{r} = (x, y)$. The target is modeled as a simple-shaped PEC object in the shadow region illustrated as the region painted gray in Fig. 2. The antenna is used for both transmitting and receiving, and is scanned along a straight line. The i-th antenna location is expressed as $x = i\Delta x + x_0$, where Δx is the interval of the antenna location. The antenna scans along a line $y = y_0$ in the x direction. Raised-cosine-shaped UWB pulses, with a center frequency of 79 GHz and a bandwidth of 1.4 GHz, are transmitted and echoes are received by the same antenna. The antenna is assumed to have an ideally uniform beam pattern with a beam width of 180° and with the main lobe in the direction of the y-axis. We define $s'(X, Z)$ as the received signal at the antenna location $\boldsymbol{r} = (X, y_0)$, where we define Z in terms of time t and the speed of the radiowave c as $Z = \mathrm{c}t$. The ray tracing method [13], [14] is used to calculate the received signal. In this method, the propagation of electric waves is modeled with multiple straight lines; the received signal is calculated as the summation of all the components of the paths. The signal $s'(Z)$ received at $\boldsymbol{r} = (X, y_0)$ is calculated as

$$s'(Z) = \sum_n A_n w(Z - \mathrm{c}\tau_n), \tag{1}$$

where n is the number of paths from the antenna to the target, A_n and τ_n represent the amplitude and relative delay of the n-th component, and $w(Z)$ is the reference waveform. The undesired direct reflections including direct crosstalk are subtracted from the received data. To subtract these from the data measured in an actual environment with a target, the direct echoes from the walls are measured in advance. The direct echoes should be measured periodically because the environment can change over time. A filter matched to a transmitted waveform is applied to the raw signal $s'(X, Z)$ to obtain a filtered signal $s(X, Z)$. The imaginary space expressed with (X, Z) is called the data space.

For convenience, we introduce mirror image antennas that are located at symmetrical positions with respect to the room walls as in Fig. 3. Each multipath wave can be modeled with an imaginary echo from the corresponding mirror image antenna. These mirror image antennas can be treated as the actual antennas, aside from the reflection coefficient of the walls involved. The j-th mirror image antenna for the i-th antenna position is located at $\boldsymbol{a}_i^{(j)} = (x_i^{(j)}, y_i^{(j)}) = (i\Delta x^{(j)} + x_0^{(j)}, y_0^{(j)})$ $(i = 0, \cdots, M; j = 0, \cdots, N)$, where M is the number of antenna locations, N is the number of mirror image antennas, and $\Delta x^{(j)}$ is the interval of the j-th mirror image antenna's location. In the case $j = 0$, it represents an actual antenna location.

III. Conventional Method

A. SEABED Method

A high-speed UWB radar imaging method, SEABED [5] has been proposed based on a simplified target model. This method uses a reversible boundary scattering transform (BST) between the point in real space (x, y) and the point in data space (X, Z'), which is extracted from the output of the matched filter $s(X, Z)$, where $Z' = Z/2$. The inverse BST (IBST) is expressed as

$$\begin{cases} x = X - Z'\,\mathrm{d}Z'/\mathrm{d}X, & (2)\\ y = Z'\sqrt{1 - (\mathrm{d}Z'/\mathrm{d}X)^2}, & (3)\end{cases}$$

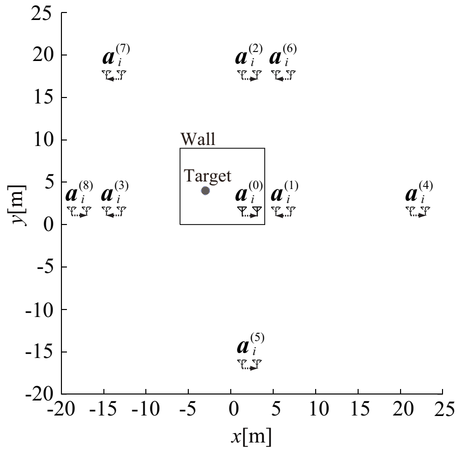

Fig. 4. System model B without shadow regions.

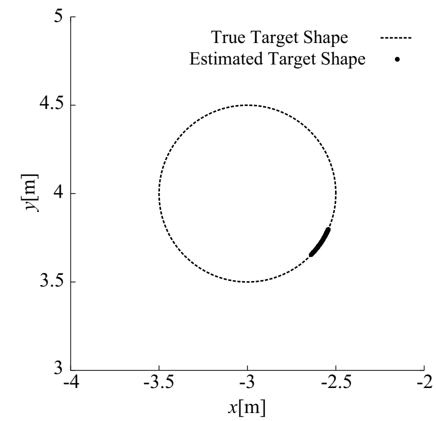

Fig. 5. Image estimated by the SEABED method.

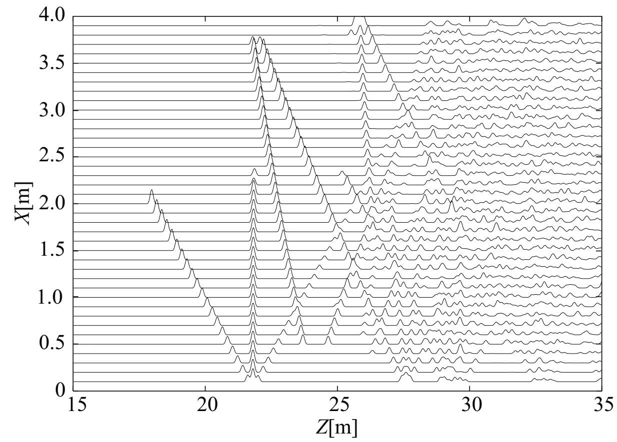

Fig. 6. Received signals after applying the matched filter.

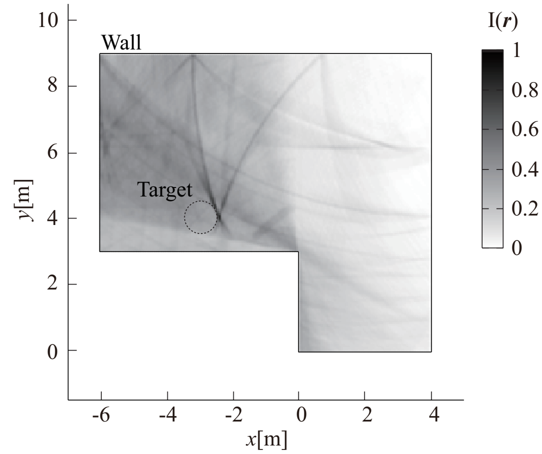

Fig. 7. Image estimated by the TR method.

where $|\mathrm{d}Z'/\mathrm{d}X| \leq 1$ holds. Although it is reported that the SEABED method can obtain a high-quality image, this method can be applied only to measurements using direct echoes received without any multipath signals as in Fig. 4.

Figure 5 shows the estimated image by applying the IBST to the system model shown in Fig. 4. Here, a circular target with a radius of 0.5 m located at $(-3.0\,\mathrm{m}, 4.0\,\mathrm{m})$ is assumed. We also set the other parameters $(x_0, y_0) = (0.1\,\mathrm{m}, 1.0\,\mathrm{m})$, $\Delta x = 0.1\,\mathrm{m}$, and $M = 38$. In Fig. 5, although SEABED provides an accurate target shape, we can obtain only a small part of it because we use only direct echoes from the target without any multipath echoes.

B. Time-Reversal Imaging Method

The time reversal (TR) method is another approach to UWB radar imaging that is likely to be applicable even to multipath echoes [11]. In the TR method, extended to shadow region imaging, the image $I(\boldsymbol{r})$ is formulated as

$$I(\boldsymbol{r}) = \sum_i \sum_{p=0}^{N} \sum_{q=0}^{N} H(p, q, \boldsymbol{r}) \left| s'\left(X, \left|\boldsymbol{r} - \boldsymbol{a}_i^{(p)}\right| + \left|\boldsymbol{r} - \boldsymbol{a}_i^{(q)}\right|\right)\right|^2, \quad (4)$$

where $H(p, q, \boldsymbol{r})$ is the function defined as

$$H(p, q, \boldsymbol{r}) = \begin{cases} 1 & (\boldsymbol{r} \notin \boldsymbol{\Pi}_p \cup \boldsymbol{\Pi}_q), \\ 0 & (\boldsymbol{r} \in \boldsymbol{\Pi}_p \cup \boldsymbol{\Pi}_q). \end{cases} \quad (5)$$

In Eq. (5), $\boldsymbol{\Pi}_p$ is the shadow region from the location of the p-th antenna. Equation (4) indicates that the image $I(\boldsymbol{r})$ is produced by summing all the signals using different antenna pairs after compensating for the time delay. The function $H(p, q, \boldsymbol{r})$ prevents the summation from including contradictory components that propagate through the PEC walls.

We apply this method to the system model shown in Fig. 3. Figure 6 shows the received signals $s(X, Z)$ for the system model in Fig. 3. Here, the observation time is $0 \leq t \leq 150\,\mathrm{nsec}$, corresponding to a range of 45 m. We assume $N = 6$, which means that the image is produced with multipath echoes with the number of reflections less than or equal to three.

Figure 7 shows the image obtained by the TR method. The image is normalized using the maximum value of $I(\boldsymbol{r})$. In this figure, although the target location is estimated, a target shape cannot be seen, meaning that this method cannot be used for radar imaging in multipath environments.

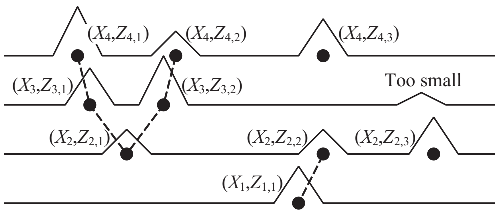

Fig. 8. Schematic of extracting pairs of range points.

IV. Proposed Method

A. Extraction of Range Point Pairs

This section describes the proposed imaging algorithm for obtaining high-resolution images in an indoor environment. In this subsection, we explain the procedure for the initial data processing of the received signals. $(X_i, Z_{i,k})$ is defined as a range point that is extracted from the peak points of $s(X,Z)$ as

$$\delta\, s(X,Z)/\delta Z = 0, \tag{6}$$

$$s(X,Z) \geq \rho \max s(X,Z), \tag{7}$$

where X_i is the i-th actual location of an antenna and $Z_{i,k}$ is the k-th peak of the signal received at (X_i, y_0). The parameter $\rho \geq 0$ is empirically determined. The peak points are extracted by finding the local maximum points with the quasi-Newton method. Only the signal satisfying Eq. (7) is the target for this search. The initial values for the search are set to $m\Delta Z_s$, where $m\Delta Z_s$ satisfies the condition:

$$s(X_i, m\Delta Z_s) = \max\left\{s(X_i,(m-1)\Delta Z_s),\, s(X_i, m\Delta Z_s),\, s(X_i,(m+1)\Delta Z_s)\right\}. \tag{8}$$

ΔZ_s is the sampling interval of Z. The sampled data of the signal $s(X,Z)$ is interpolated using the sinc function in this search. Moreover, we pick up pairs of adjacent range points satisfying the condition

$$|Z_{i,u} - Z_{i+1,v}| \leq T_0, \tag{9}$$

where T_0 is the length of the transmitted pulse. The schematic for this procedure is illustrated in Fig. 8. We set $T_0 = 0.2\,\mathrm{m}$ for the assumed system model using a pulse with a bandwidth of 1.4 GHz. The black dots connected with solid lines in Fig. 9 show the pairs of range points extracted by the procedure described above, where we set $\rho = 0.5$.

B. Interferometry Imaging in an Indoor Environment

In this subsection, we describe the proposed imaging method using the range points extracted in the previous subsection. Note that the received echoes include both monostatic and bistatic radar echoes. If the transmitting and receiving propagation paths are identical, as in the left-hand part of Fig. 10, this is interpreted as a monostatic radar signal with a single actual/imaginary antenna. In contrast, other reflected echoes propagate along a path different from the transmitting propagation path. This echo corresponds to a bistatic radar arrangement as in the right-hand part of Fig. 10.

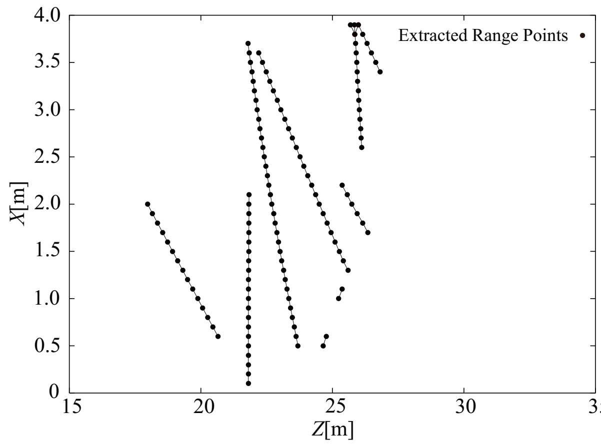

Fig. 9. Extracted pairs of range points.

The interferometry method [12] is employed for imaging using the extracted pairs of range points. Interferometry is a commonly used technique for direction-of-arrival (DOA) estimation using the phase difference between multiple echoes received with different antennas. By extending this principle, the target shape is provided by solving the intersection points of the following two ellipses:

$$\begin{cases} \left|\boldsymbol{r} - \boldsymbol{a}_i^{(p)}\right| + \left|\boldsymbol{r} - \boldsymbol{a}_i^{(q)}\right| = Z_{i,u}, & (10) \\ \left|\boldsymbol{r} - \boldsymbol{a}_{i+1}^{(p)}\right| + \left|\boldsymbol{r} - \boldsymbol{a}_{i+1}^{(q)}\right| = Z_{i+1,v}. & (11) \end{cases}$$

This can be used for estimating the DOA by measuring the difference between the delays of the multiple echoes received by different antennas. In the case $p = q$, as shown in the left-hand part of Fig. 10, the solution is given by the intersection of two circles rather than ellipses. The schematic of this interferometry method is illustrated in Fig. 11, where an ellipse with foci $\boldsymbol{a}_i^{(1)}$ and $\boldsymbol{a}_i^{(2)}$, and another ellipse with foci $\boldsymbol{a}_{i+1}^{(1)}$ and $\boldsymbol{a}_{i+1}^{(2)}$ are used to calculate the target location. We apply these methods to all possible combinations of pairs of range points and antennas to obtain an estimated image. Finally, if the estimated point falls outside the room, the point is removed.

The image estimated by this method is shown in Fig. 12, where a broken line and the black dots represent the actual target shape and the estimated image respectively. Although this image is a correct estimate of the circular target, it also has many false image points because it contains incorrect combinations of a range of points and antennas. This is because incorrect pairs of antennas and range points are used to produce the image.

C. False Image Reduction Method

The problem is that we cannot know which echo corresponds to which pair of antennas at this stage. First, we calculate a rough image using the conventional TR method to estimate the approximate location of targets as in Fig. 7. We estimate the maximum point $\boldsymbol{r}_{\max}$ from the image in Fig. 7. Next, we pick up consistent combinations of range points that

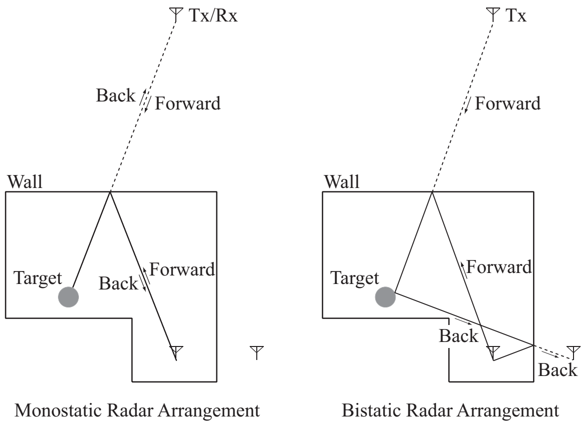

Fig. 10. Two types of propagation paths.

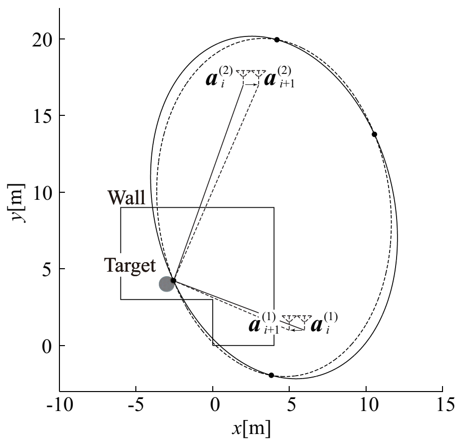

Fig. 11. Schematic of bistatic interferometry.

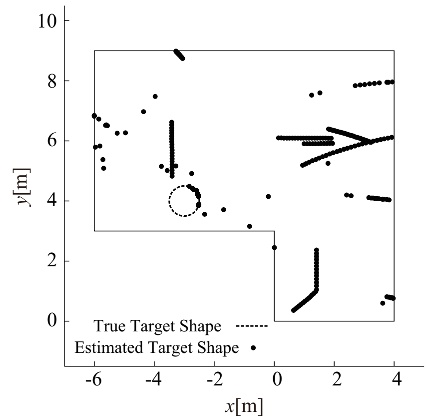

Fig. 12. Estimated image points without false image reduction process.

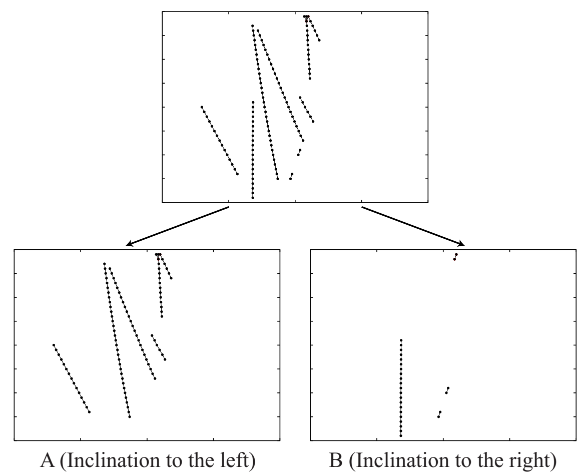

Fig. 13. Schematic of false image reduction process.

satisfy the relationship between the actual/imaginary antenna scanning direction and the estimated range values. We only use antenna pairs based on the inclination of the lines connecting the range points. In this process, echoes are divided into two groups A and B as in Fig. 13. Each antenna pair is classified as a member of either group A or group B. Applying the interferometry method, we add the following condition:

$$\begin{cases} Z_{i,u} \geq Z_{i+1,v} & \left(\left|\boldsymbol{r}_{\max} - \boldsymbol{a}_i^{(p)}\right| + \left|\boldsymbol{r}_{\max} - \boldsymbol{a}_i^{(q)}\right| \right. \\ & \left. \geq \left|\boldsymbol{r}_{\max} - \boldsymbol{a}_{i+1}^{(p)}\right| + \left|\boldsymbol{r}_{\max} - \boldsymbol{a}_{i+1}^{(q)}\right|\right), \quad (12) \\ Z_{i,u} < Z_{i+1,v} & \left(\left|\boldsymbol{r}_{\max} - \boldsymbol{a}_i^{(p)}\right| + \left|\boldsymbol{r}_{\max} - \boldsymbol{a}_i^{(q)}\right| \right. \\ & \left. < \left|\boldsymbol{r}_{\max} - \boldsymbol{a}_{i+1}^{(p)}\right| + \left|\boldsymbol{r}_{\max} - \boldsymbol{a}_{i+1}^{(q)}\right|\right). \quad (13) \end{cases}$$

In addition, we assume that true image points exist within the vicinity of the point $\boldsymbol{r}_{\max}$ for $|\boldsymbol{r} - \boldsymbol{r}_{\max}| < \mu$.

The target shape estimated by the proposed method is shown in Fig. 14, where the white square symbol represents the estimated target location $\boldsymbol{r}_{\max}$, and where we set $\mu = 0.5\,\mathrm{m}$ and $\boldsymbol{r}_{\max} = (-2.40\,\mathrm{m}, 4.10\,\mathrm{m})$. In this figure, most of the false images are removed and the true target shape is accurately estimated. Compared with the image estimated by the TR method shown in Fig. 7, the proposed method provides more significant images for recognizing the target shape with a clear surface. The RMS error of the estimated shape is 0.47 mm. Of course, this error is not realistic because a noiseless environment is assumed here. We analyze the performance in a noisy environment in the next section. Note however that the bandwidth and center frequency have much to do with the estimation accuracy and the width of the estimated region. If the bandwidth is narrower, there can be more interference in the received signals, which deteriorates the accuracy of the estimated image as the extracted peak points include range errors. Moreover, the reflection coefficient changes with center frequency. If the reflection coefficient is smaller, the number of usable range points decreases for the conditional equation shown in Eq. (7), which causes the diminution of the estimated region.

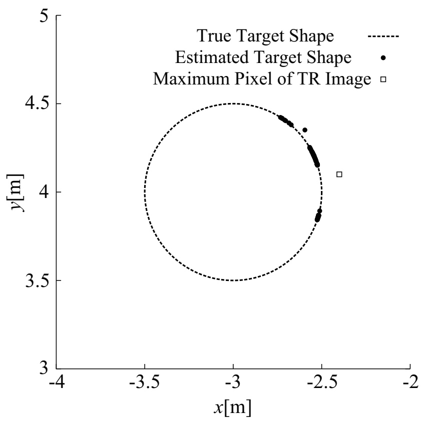

Fig. 14. Estimated image points with false image reduction process.

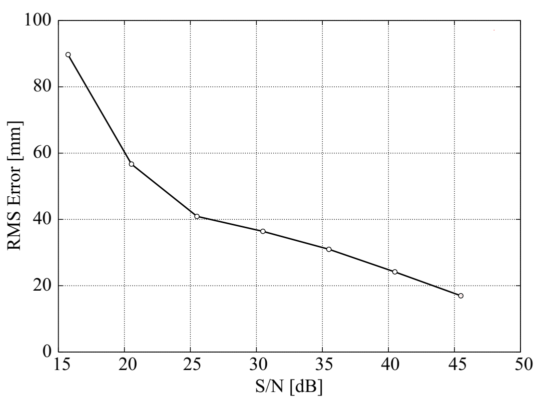

Fig. 15. RMS error of the proposed method vs. S/N.

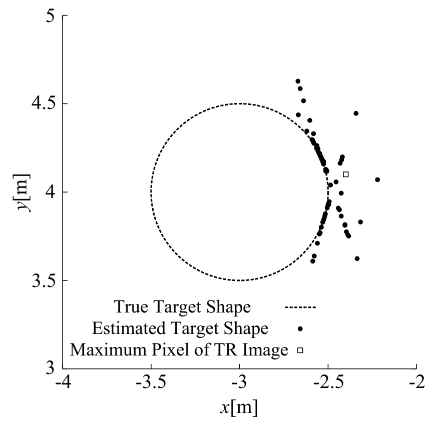

Fig. 16. Estimated image points for S/N=30.50 dB.

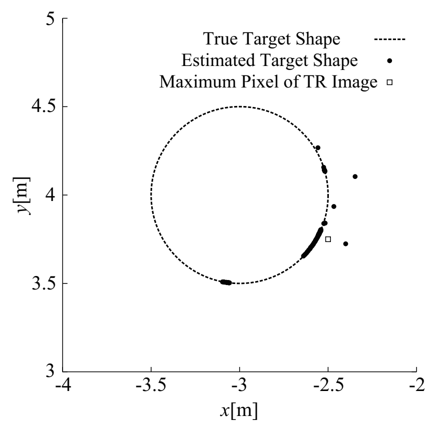

Fig. 17. Estimated image points for a target in a line-of-sight area.

V. Performance Evaluation of the Proposed Method

A. Noise Tolerance

Assuming the same scenario as in the previous section, we show the imaging accuracy of the proposed method with noisy data. To produce a noisy signal numerically, white Gaussian noise is added to the raw signals $s'(X, Z)$. We define S/N as the ratio of the peak instantaneous signal power to the averaged noise power after applying the matched filter. The RMS error of the estimated shape using the proposed method is shown in Fig. 15. This figure shows that the RMS error is relatively small, at less than 40 mm for S/N $\geq$ 25.50 dB. The TR method provides an accurate estimation of $\boldsymbol{r}_{\max}$ for S/N $\geq$ 15.73 dB, whereas the interferometry method fails to estimate accurate image points for S/N $\leq$ 25.50 dB. We have confirmed that the image estimated by the TR method cannot estimate an accurate target location, leading to a poor performance of the proposed method. Therefore, the proposed method requires S/N to be larger than 25.50 dB. The image estimated in noisy environments is shown in Fig. 16 for S/N = 30.50 dB. In Fig. 16, although there are inappropriate false points, most of the estimated points are located on the target surface, giving an accurate image estimation.

B. Performance Evaluation with Other Models

This subsection discusses the performance of the proposed method with different models. First, we apply the proposed method to model B shown in Fig. 4. The target image obtained is shown in Fig. 17. This result verifies that the region containing images is extended compared with Fig. 5 because the proposed method uses not only the direct echo but also multipath echoes for imaging. The estimation RMS error is 1.78 mm.

Next, we show the performance of the proposed method assuming the environment shown in Fig. 18, modeling the corner of a hallway. The estimated image is shown in Fig. 19. In this figure, a different part of the target boundary is accurately estimated. The estimation RMS error is 33.19 mm.

Finally, we apply the proposed method to an elliptical PEC target in model A shown in Fig. 3. Figure 20 shows an example of the estimated image for the target with an inclination angle of 120°, where part of the target shape is correctly estimated with an estimation RMS error of 0.02 mm. We have also applied the proposed method to the same elliptical targets with various inclination angles over the range $60^\circ \leq \psi \leq 120^\circ$ and confirmed the average estimation RMS error to be 2.57 mm.

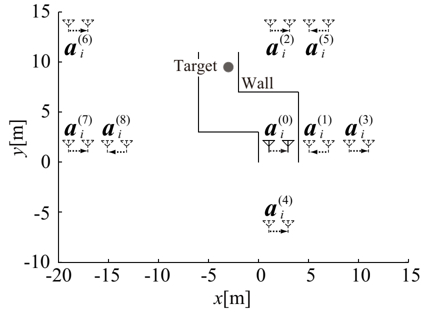

Fig. 18. System model C for a hallway.

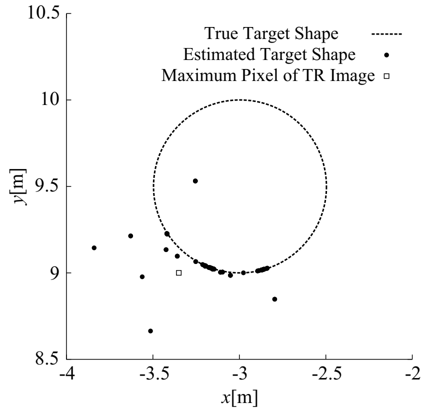

Fig. 19. Image estimated for system model C.

VI. Conclusions

This paper proposes an imaging method for a target in a shadow region using a single antenna. First, we established that conventional methods do not provide sufficient resolution of a target in a shadow region. To obtain a high-resolution image, we proposed an imaging method using the principle of interferometry and applied this method to each of the mirror image antennas. In addition, we proposed a false image reduction algorithm using an approximate target location obtained by the TR method and the inclination of the estimated pairs of echoes in the data space. In this process, most of the false image points were removed and the target boundary was estimated accurately. We also investigated the performance of the proposed method for noisy data and clarified that an accurate image is obtained when S/N is higher than about 25 dB. Moreover, we investigated the performance of the proposed method in different system models, confirming the effectiveness of the proposed method in a variety of situations. However, we only investigated the performance evaluation of the proposed method by the restricted ideal system model. In an actual indoor environment, some additional factors adversely affect the performance of our proposed algorithm, such as clutters, interference, antenna radiation pattern nulls, polarization mismatch, and dynamic range. Furthermore, targets and walls are not made of PEC in an actual environment, and since S/N is lower than in the ideal environment the

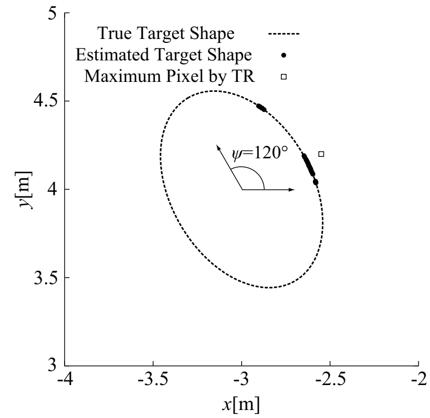

Fig. 20. Estimated image points for an elliptical target.

estimation accuracy is also lower and the estimated region is diminished. These are issues to be addressed in the future.

References

[1] S. Ikeda, H. Tsuji, and T. Ohtsuki, "Indoor event detection with Eigenvector spanning signal subspace for home or office security," IEICE Trans. Commun., vol. E92-B, pp. 2406–2412, 2009.

[2] K. Pahlavan, F. O. Akgul, M. Heidari, A. Hatami, J. M. Elwell, and R. D. Tingley, "Indoor geolocation in the absence of direct path," IEEE Wireless Communications, vol. 13, no. 6, pp. 50–58, 2006.

[3] C. Le, T. Dogaru, L. Nguyen, and M. R. Ressler, "Ultra wideband (UWB) radar imaging of building interior: Measurements and predictions," IEEE Trans. Geosci. Remote Sens., vol. 47, no. 5, pp. 1409–1420, 2009.

[4] X. Zhuge, T. G. Savelyev, A. G. Yarovoy, and L. P. Ligthart, "UWB array-based radar imaging using modified Kirchhoff migration," 2008 IEEE International Conference on Ultra-WideBand (ICUWB2008), vol .3, pp. 175–178, 2008

[5] T. Sakamoto, "A fast algorithm for 3-D imaging with UWB pulse radar systems," IEICE Trans. Commun., vol. E90-B, pp. 636–644, 2007.

[6] S. Kidera, Y. Kani, T. Sakamoto, and T. Sato, "A fast and high-resolution 3-D imaging algorithm with linear array antennas for UWB pulse radars," IEICE Trans. Commun., vol. E91-B, no. 8, pp. 2683-2691, 2008

[7] T. Sakamoto, Y. Matsuki and T. Sato, "A novel UWB radar 2-D imaging method with a small number of antennas for targets with arbitrary shapes and motion," 2009 IEEE International Conference on Ultra-WideBand (ICUWB2009), pp. 9-11, 2009.

[8] E. A. Marengo and F. K. Gruber, "Subspace-based localization and inverse scattering of multiple scattering point targets," EURASIP J. Appl. Signal Process., vol. 2007, pp. 192–192, 2007.

[9] Y. Jin and J. M. E. Moura, "Time-reversal detection using antenna arrays," IEEE Trans. Signal Process., vol. 57, pp. 1396–1414, 2009.

[10] T. Sakamoto and T. Sato, "Time-reversal UWB imaging with a single antenna in multi-path environments," 3rd European Conference on Antennas and Propagation (EuCAP) 2009, pp. 23–37, 2009.

[11] T. Sakamoto and T. Sato, "A method of estimating a room shape with a single antenna in a multipath environment," 4th European Conference on Antennas and Propagation (EuCAP) 2010, pp. 12–16, 2010.

[12] D. Massonet and K. L. Feigl, "Radar interferometry and its applications to changes in Earth's surface," Rev. Geophys., vol. 36, no. 4, pp. 441–500, 1998.

[13] M. F. Iskander and Z. Yun, "Propagation prediction models for wireless communication systems," IEEE Trans. Microwave Theory Tech., vol. 50, pp. 662–673, 2002.

[14] M. C. Lawton and J. P. McGeehan, "The application of a deterministic ray launching algorithm for the prediction of radio channel characteristics in small-cell environments," IEEE Trans. Veh. Technol., vol. 43, pp. 955–968, 1994.